Anti-Stokes Photoluminescence in Nanocrystal Quantum Dots

ARTICLE *in* THE JOURNAL OF PHYSICAL CHEMISTRY B · JULY 2002

Impact Factor: 3.3 · DOI: 10.1021/jp0208743

3 AUTHORS, INCLUDING:

Noelio Oliveira Dantas
Universidade Federal de Uberlândia (UFU)
149 PUBLICATIONS **1,013** CITATIONS
SEE PROFILE

Fanyao Qu
University of Brasília
96 PUBLICATIONS **911** CITATIONS
SEE PROFILE

Anti-Stokes Photoluminescence in Nanocrystal Quantum Dots

Noelio Oliveira Dantas, Fanyao Qu,* and R. S. Silva

Universidade Federal de Uberlândia, Faculdade de Física, Laboratório de Novos Materiais Isolantes e Semicondutores, C.P. 593, CEP 38400-902, Uberlândia (MG), Brazil

Paulo César Morais

Universidade de Brasília, Instituto de Física, Núcleo de Física Aplicada, C.P. 04455, CEP 70919-970, Brasília (DF), Brazil

Received: April 3, 2002

In this study the fusion method was used to synthesize PbS nanocrystal quantum dots (QDs) embedded in S-doped glass matrix ($SiO_2-Na_2CO_3-ZnO-Al_2O_3-PbO_2-B_2O_3$). Optical absorption, atomic force microscopy (AFM), and photoluminescence (PL) were used to investigate different samples. Experimental data indicate that the PbS QD-size is controlled by the different annealing times the S-doped glass matrix is submitted to. The size-dependence of the optical transitions in PbS QDs were obtained by numerical calculation and compared with the experimental data. A strong anti-Stokes photoluminescence (ASPL), from green (2.409 eV) to violet (2.978 eV), was found in all samples, at room temperature. A possible microscopic mechanism leading to the ASPL, which involves a two-photon absorption in two separate steps through a surface state, is proposed.

1. Introduction

Semiconductor lasers have been widely used in telecommunications, information storage, medical diagnostics, and therapeutics, among others. Quantum well (QW) lasers represented an important step forward in the semiconductor laser technology. Quantum confinement of carriers in a QW structure enhances the electron−hole wave function overlap, increases the transition oscillator strength, and pushes the density of states toward the band edge, which favors excitonic transitions. Consequently, the lasing threshold is reduced, the temperature stability is improved, and the QW laser line is narrowed.[1−3] Owing to a further enhancement of the density of states at the band edge, nanocrystal quantum dots (QDs) exhibit a variety of novel and interesting optical properties.[4,5] For instance, QD array lasers lost temperature sensitivity, increased orders of magnitude in gain, showed reduction in the threshold current, line width and noise, and increased nonlinear gain.[6] Due to the large exciton Bohr radius (200 Å), PbS nanocrystal QDs provide unique access to the limit of strong quantum confinements and thus offer excellent opportunities for both experimental and theoretical investigations, as far as the properties of a size-quantized system is concerned.[7] The PbS band-gap can be tuned from the infrared up to the near-ultraviolet region, depending only upon the nanocrystallite size. Actually, a tunneling of the optical band-gap of PbS QDs, from 0.41 eV (bulk material) to about 5.2 eV (small QDs) has been already achieved.[8] Finally, PbS QDs show absorption peaks in the 1−2 μm (0.6−1.3 eV) range, which is extremely important for the telecommunication industry.[7]

Whereas optical absorption represents a traditional technique in the investigation of low-dimensional semiconductor structures, anti-Stokes photoluminescence (ASPL) has recently attracted a great deal of attention. Shortly, in the ASPL the optical emission occurs at energy larger than the energy of the excitation source. This effect has been previously reported in bulk semiconductors,[9] one-dimensional crystalline semiconductor heterostructures,[10,11] and quantum wells.[12,13] Two-photon absorption process, thermal activation by Auger transitions, and absorption of phonons are three plausible microscopic mechanisms leading to ASPL. In the first one two photons are absorbed sequentially in two separate steps (TS−TPA) through a deep/shallow impurity state.[10,14] The second one is an Auger-like recombination, in which an electron−hole pair decays nonradiatively while the energy is used to excite another electron or hole into higher energy states.[15] The third one involves absorption of LO phonons, which is described by the Fröhlich interaction.[5] Very recently, InAs/GaAs[16] and InP/GaInP[17] self-assembled QDs and InP and CdSe colloidal QDs[18] have been investigated by ASPL. In InAs QDs embedded in GaAs the ASPL data are explained by a TS−TPA process involving quantum dot states.[16] However, in InP/GaInP QDs (self-assembled and colloidal) the TS−TPA processes, involving either deep energy levels localized close to the QDs[17] or the surface states near the valence band and conduction band edges,[18] was used to explain the experimental data. Up to date, however, ASPL in PbS nanocrystal QDs has not been reported. In this study, PbS nanocrystal QDs were synthesized in oxide glasses and systematically investigated by means of optical absorption, photoluminescence (PL), anti-Stokes photoluminescence, and atomic force microscopy (AFM). Further, theoretical calculations based on the four-band envelope-function formalism, were carried out and compared with the experimental data.

2. Sample Preparation and Experimental Details

The sulfur-doped oxide glass matrix ($SiO_2-Na_2CO_3-ZnO-Al_2O_3-PbO_2-B_2O_3$) used in this study was prepared from high purity powders using SiO_2 as glass former, ZnO as intermediate oxide, and Na_2CO_3 to reduce the melting point. The mixture was melted in an aluminum crucible at 1400 °C, for 2 h. Then,

* To whom correspondence should be addressed. Phone: (+55-34) 3239-4190. Fax: (+55-34)32394106. E-mail: fanyao@ufu.br.

10.1021/jp0208743 CCC: $22.00
Published on Web 07/09/2002

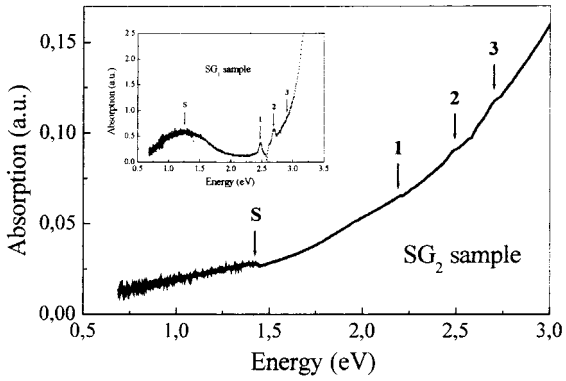

Figure 1. Room-temperature optical absorption spectrum of sample SG_2 (3 h annealing time). The insert shows the optical absorption spectrum of sample SG_1 (1 h annealing time). Arrows indicate optical absorption peaks.

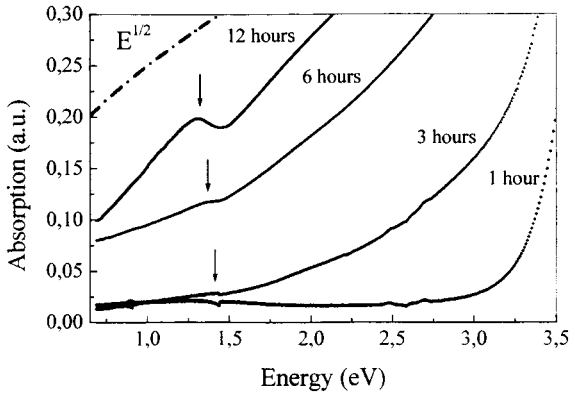

Figure 2. Room-temperature optical absorption spectra of samples SG_1, SG_2, SG_3, and SG_4, annealed at 600 °C during 1, 3, 6, and 12 h, respectively. The dash−dotted line ($E^{1/2}$) represents the optical absorption spectrum of bulk PbS.

it was fast cooled to room temperature. To release thermal stresses, the glass matrix was first annealed at 350 °C, for 3 h. A second thermal treatment of the glass matrix was performed at 600 °C, to enhance the diffusion of Pb^{2+} and S^{2-} ions. As a result of the second thermal treatment PbS, QDs were formed in the glass matrix. Two sets of samples were prepared. In the first set of samples the annealing times were 1, 3, 6, and 12 h. The samples were labeled SG_1, SG_2, SG_3, and SG_4 according to the annealing time of 1, 3, 6, and 12 h, respectively. This leads to their coloring varying from brown to black, depending on the exact duration of annealing. In the second sample preparation the annealing times were 5 and 30 h and the samples were labeled AFM_1 and AFM_2, respectively. Samples SG_1, SG_2, SG_3, and SG_4 were cut and polished for optical measurements. The optical measurements were recorded using a SPEX-750M monochromator equipped with a Joban-Yvon CCD 2000 × 800−3. The samples were optically excited using the 514.5 nm Argon-ion laser line. Samples AFM_1 and AFM_2 were prepared to take the AFM images.

3. Results and Discussion

Figure 1 shows the absorption spectrum taken from the SG_2 sample (3 h annealing time), in the spectral range 0.5−3.0 eV. The insert shows the absorption spectrum of the SG_1 sample (1 h annealing time) in the same spectral range. Both samples present four well-resolved optical features, indicated in Figure 1 as S, 1, 2, and 3. Energy position of the optical features were found at 1.391 (1.420), 2.486 (2.200), 2.691 (2.490), and 2.894 (2.863) eV for the sample SG_1 (SG_2), respectively. However, it is also found in both cases that the absorption peak S is broader than features 1, 2, and 3. Such a difference can be explained by assuming that feature *S* originates from surface sates, whereas features 1, 2, and 3 are attributed to intrinsic QD transitions. Broadening of the S peak is explained in terms of scattering processes introduced by localized phonons in surface defects.

Figure 2 shows the effect of the annealing time upon the absorption spectra, for samples SG_1, SG_2, SG_3, and SG_4. Note that (see Figure 2) an increase in the annealing time leads to a red shift of the optical features (1, 2, and 3), thus suggesting an increase in QD-size. In contrast, feature S does not shows any significant energy shift upon annealing, though intensity and broadening enhancement are observed. Such observation provides a strong support to the origin of feature S, as mentioned previously. With increasing annealing time (and the assumed increasing in QD-size) the ground state energy reduces and so the energy differences between atomic-like QD states. Thus, the surface state and the ground QD state energies tend to merge together. In larger QDs, even excited QD states are very much close in energy to the surface state. As a result, the individual optical features are not easily resolved. Therefore, the *S* feature becomes broad with increasing annealing time. It is needless to mention that the optical absorption spectrum depends on the concentration of the PbS QD in the glass matrix, the properties of the glass matrix itself, and the details of the annealing procedure.

Comparison between the data obtained from numerical calculation of the energy levels and the energy associated to the features observed in the optical absorption spectra can be used to estimate the PbS QD sizes. A simple numerical calculation is based on the solution of the single-particle Schrödinger equation, assuming infinite potential well and parabolic energy bands. Figure 3a shows the calculated transition energies in PbS QD as a function of the QD size. The effective electron (hole) mass used in the calculation was $m_e^* = 0.25\, m_0$ ($m_h^* = 0.25 m_0$), where m_0 is the free electron mass. A more sophisticated calculation was also performed by means of the four-band envelope-function formalism based on a bulk $(4\times4)\mathbf{k}\cdot\mathbf{p}$ Hamiltonian. The calculated transition energies are shown in Figure 3b. Since the band parameters in PbS QDs are almost isotropic, the effects of band anisotropy in the calculation of the transition energies have been neglected.[19,20] The eigenvalues resulting from the $\mathbf{k}\cdot\mathbf{p}$ method are labeled by the corresponding angular momentum quantum number (j) and parity (π). Note that the transition energies associated to the ground and first excited states in Figure 3a agree very much with the values presented in Figure 3b. Further, in the strong confinement regime (QD size ≤ 80 Å) the transition energies decrease very quickly as the QD radius increases. However, in the range of dot size larger than 100 Å the size dependence of electron and hole subband energies becomes weaker. Moreover, the energy spacing between electron (hole) states becomes smaller than the room temperature thermal energy. An important consequence of that is the breakdown of the phonon bottleneck in wider QDs, resulting in temperature-dependent lasing characteristics. Finally, the QD size of PbS immersed in silicate glass can be estimated by comparing the calculated transition energy with the optical absorption features. For instance, the calculated value for the first optical transition of a 24 Å PbS QD is 2.44 eV, which is very much close to the optical feature 1 (2.48 eV) of sample SG_1. Thus, the average PbS QD size in sample SG_1 is about 24 Å. Likewise, it is possible to estimate the average sizes of PbS QDs in samples SG_2 and SG_3 as 27 and 40 Å, respectively.

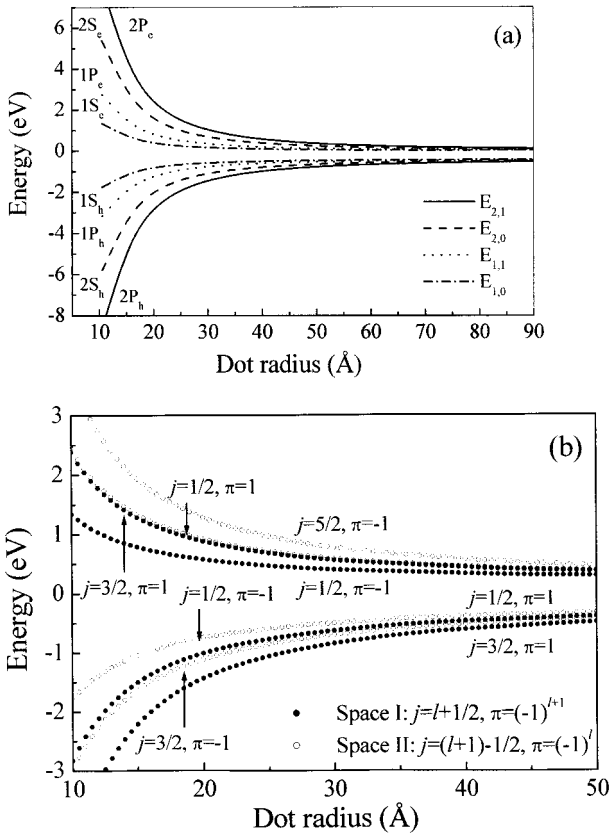

Figure 3. Calculated transition energies in PbS QD as a function of dot radius. (a) using the single-particle effective mass method in parabolic energy band approximation and (b) (4×4)**k·p** method. The eigenvalues resulting from the **k** · **p** method are labeled by the correspondent angular momentum quantum number (j) and by the parity (π), whereas l is the orbital quantum number.

Indeed, the analysis of the PbS QD-size presented above is in very good agreement with the data reported by Thielsch et al.[8]

In support to the optical absorption data and to confirm the QD formation, measurement of the average QD-size, and QD size-distribution, AFM images were taken, as shown in Figure 4. The upper part of Figure 4a shows the AFM image of sample AFM_1 (5 h annealing time), in a 5 × 5 μm^2 scan. The lower part of Figure 4a shows a detail of the AFM image as indicated by the selected square spot (see upper part) as well as the correspondent QD-size distribution. Figure 4b shows a detail of the AFM image of sample AFM_2 (30 h annealing time) and the correspondent QD-size distribution. The first comment concerning the AFM data is that QDs have been directly observed in two samples (AFM_1 and AFM_2). The second comment concerning the AFM data is that sample AFM_1 showed a relatively narrow QD-size distribution with an average QD-size of about 40 Å. This is consistent with the optical absorption data and agrees very well with the **k·p** theoretical prediction related to sample SG_3. Further, a wider QD-size distribution was found from the AFM data of sample AFM_2. The average value of the QD-size of sample AFM_2 was about 291 Å, which is larger than the value found in sample AFM_1, as expected from the difference in annealing times.

Owing to large size distribution, low loading levels, and the poor surface passivation of QDs embedded in glass matrix, which leads to high rates of surface trapping and, consequently, to large nonradiative carrier losses, the stimulated emission is often difficult to be observed.[6] Nevertheless, adequate control of both growth conditions and annealing time allows observation of stimulated emissions from QDs embedded in glass matrix. Figure 5 shows the luminescence spectra of the four synthesized samples (SG_1, SG_2, SG_3, and SG_4). Note that ASPL emission, from green (2.409 eV) to violet (2.978 eV), was observed in all samples. Further, the ASPL spectra are considerably affected by the annealing procedure. As the annealing time increases the ASPL line broadens, shifts toward the lower energy side, and enhances the intensity associated to the long tail at the low energy side. Indeed, the explanation of the ASPL data in nanocrystal QDs needs to take into account all the three possible microscopic mechanisms previously mentioned.

In bulk semiconductors, carrier energy relaxation is dominated by the Fröhlich interaction with LO phonons.[5] In nanocrystal QDs, even in the regime of weak confinement, carrier relaxation mediated by interaction with phonons is hindered dramatically, because restrictions imposed by energy and momentum conservation lead to phonon bottleneck. Further reduction in the energy loss rate is expected in the regime of strong confinement, for spacing between energy levels can be much greater than required by LO phonon, and hence carrier-phonon scattering can only occur via weak multi-phonon processes. Therefore, thermal activation via absorption of phonons is certainly not a dominant anti-Stokes mechanism in the samples investigated in this study.

A possible explanation of the ASPL data, via Auger transition, has been successfully applied to systems with high carrier density. High carrier density is usually introduced via the incident laser line, at higher optical excitation intensities. An increased spatial confinement and relaxation in the translation momentum conservation in smaller QDs may lead to an increased efficiency of Auger process, in the sense of increasing an effective carrier density. On the other hand, the atomiclike structure of energy levels in nanocrystal QDs should greatly hinder Auger processes, because of the reduced availability of final states satisfying energy conservation. As a result, Auger transition is greatly restricted in the bound states of QDs.[6] The experiments were performed under low optical excitation intensities and thus the density of optically excited carriers is small. Hence, the combining effects of the above factors lead to a negligible contribution of Auger recombination to ASPL spectra. This statement is strongly supported by a sublinear ($I \sim I_{exc}^{0.86}$) rather than a superlinear excitation intensity (I_{exc}) dependence of the integrated luminescence intensity (I), as shown in Figure 6. Therefore, the mechanism leading to ASPL due to Auger recombination could be excluded from the present study.

A more plausible mechanism leading to the ASPL data, in the present study, is assigned to a TS−TPA process, in which two photons are sequentially absorbed in two separate steps. The surface states introduced by surface defects were assumed to act as intermediate states. The schematic model used to explain ASPL in PbS QDs embedded in glass matrix is shown in the insert of Figure 6. According to this model, electron−hole pairs are first created in the QD region by the optical excitation source. After the initial excitation step, electrons relax to surface states being trapped at defect sites near the QD−glass interface. Meanwhile, the holes are trapped at the QD valence band state. The second step is the excitation of the photogenerated electron from the surface state up to the QD conduction band, followed by radiative recombination of the electrons and holes across the effective QD band gap. Taking into account the uncertainty principle, a strong localization of carriers in the surface state means a wide uncertainty in momentum. Hence, the restriction of conservation of carrier momentum upon the optical transition in the second step is ruled

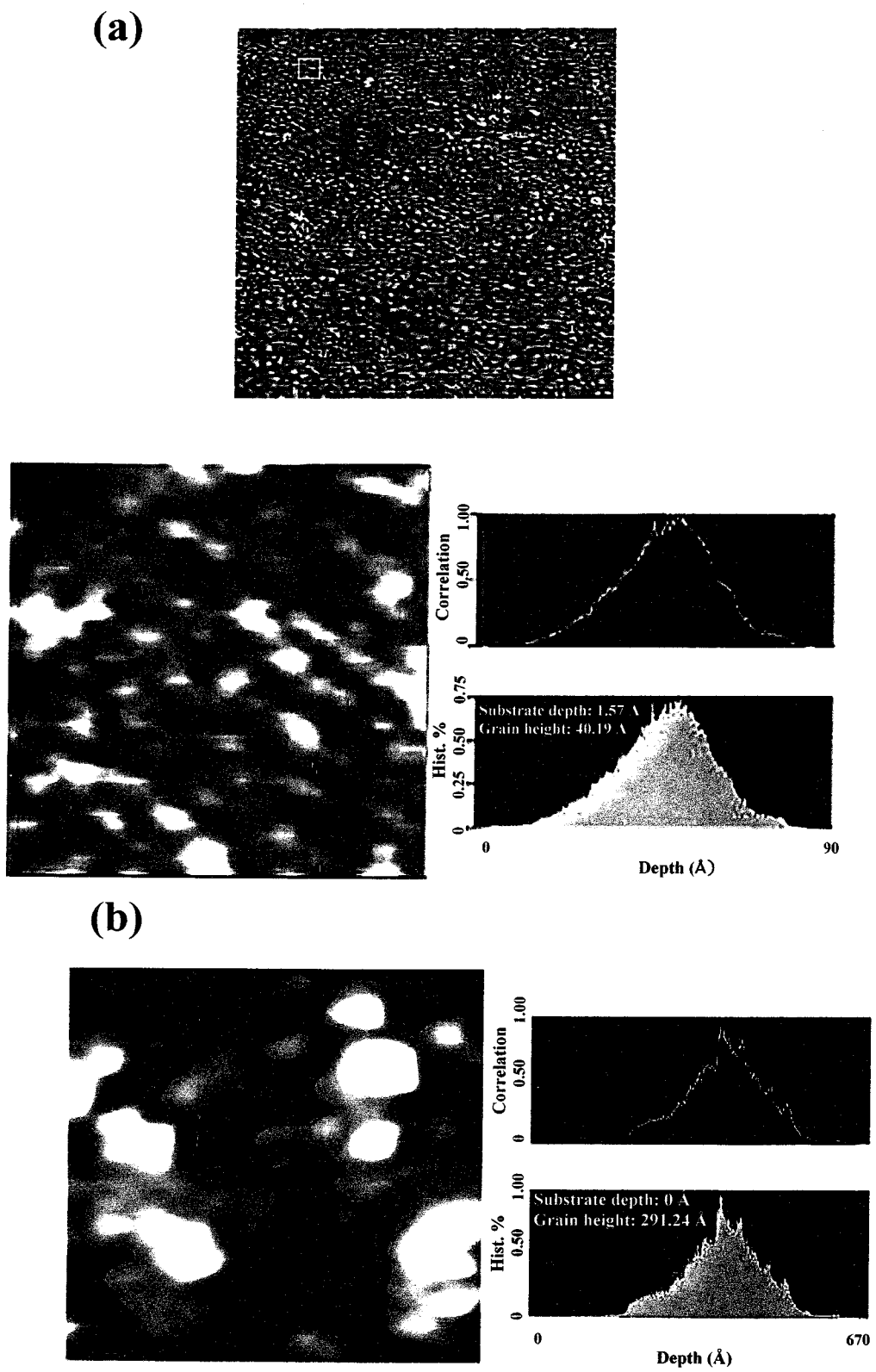

Figure 4. (a) AFM image of sample AFM_1. The upper part is the image taken in a 5×5 μm^2 scan area whereas the lower panel is a magnified image of the selected region (rectangular spot) and correspondent QD-size distribution in the spot area. (b) Magnified AFM image of sample AFM_2 and the correspondent QD-size distribution.

out. Photons required in the second absorption step can be provided either by photon direct from excitation source or by photon recycling.[21] Based on the proposed model, the sublinear behavior ($I \sim I_{exc}^{0.86}$) described in Figure 6 can be understood in terms of small density of states at the surface defect centers. In the first step of the TS−TPA-based mechanism electrons are quickly accepted at the surface defect centers, i.e., much faster than the photoionization rate of these centers in the second step.[14] Indeed, there are two points strongly supporting the model proposed for the explanation of the ASPL data: (a) the intensity of the ASPL shows sublinear power dependence upon the optical excitation intensity and (b) the ASPL occurs at transition energies which are slightly shifted in energy from one sample to another.

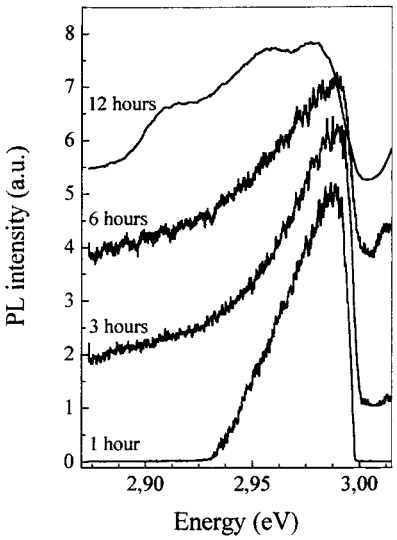

Figure 5. Room-temperature photoluminescence (PL) spectra of samples SG_1, SG_2, SG_3, and SG_4, annealed at 600 °C during 1, 3, 6, and 12 h, respectively.

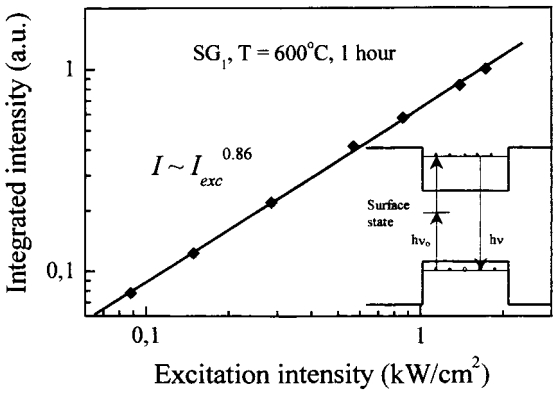

Figure 6. Integrated ASPL line intensity versus optical excitation intensity. The 514.5 nm laser line was used to excite the SG_1 sample. The solid line (slope about 0.86) shows the sublinear regression in the log−log plot. The model picture used to explain the ASPL data is schematically shown in the insert.

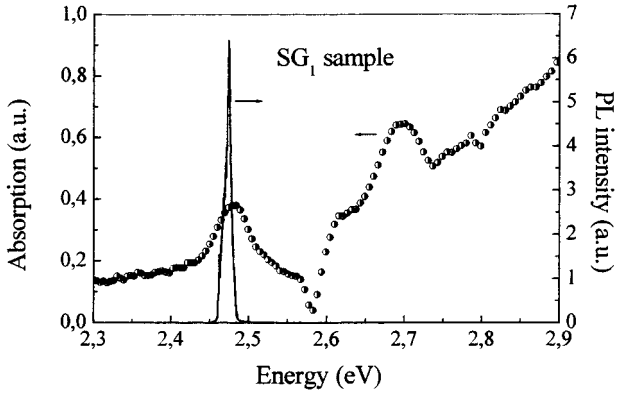

Figure 7. Optical absorption curve (symbols) and photoluminescence spectrum (solid line) for sample SG_1, scaled with the left- and right-hand side vertical axis, respectively.

In addition to the ASPL feature observed in sample SG_1 at about 2.978 eV (see Figure 5), a second up-converted emission line was observed around 2.476 eV. Figure 7 shows the optical absorption curve (symbols) as well as the photoluminescence (PL) spectrum (solid line) of sample SG_1 (1 h annealing time). Note in Figure 7 that the narrow PL line at 2.476 eV and the first absorption peak related to the intrinsic optical transition in the PbS QD are in alignment. Therefore, the observed PL line very much close to the excitation energy is more likely associated to a resonant Raman process.

4. Conclusions

Six different annealed sulfur-doped glass samples ($SiO_2-Na_2CO_3-ZnO-Al_2O_3-PbO_2-B_2O_3$) were synthesized using the fusion method. The thermal treatment the sulfur-doped glass matrix is submitted to allows the growth of PbS quantum dots whose size increases with the annealing time. An experimental investigation as well as a theoretical study related to these samples were carried out. Optical absorption features due to different optical transitions in PbS QDs embedded in glass matrix were observed. The PbS QD sizes, as predicted by theoretical analysis, are in very good agreement with the optical features observed in the absorption measurements and with the images obtained from atomic force microscopy. Anti-Stokes photoluminescence (ASPL) from green (2.409 eV) to violet (2.978 eV) was found in all samples. A plausible microscopic mechanism leading to ASPL, based on the two-step two-photon absorption process involving a QD a surface state, was proposed. A second up-converted photoluminescence line very much close to the excitation energy may originate from a resonant Raman process.

Acknowledgment. The Brazilian Agencies FAPEMIG and CNPq supported this work.

References and Notes

(1) Qu, Fanyao; Cardoso, A. J. C.; Morais, P. C. *Phys. Rev. B* **1999**, *60*, 4501.
(2) Qu, Fanyao; Dantas, N. O.; Morais, P. C. *Phys. E* **2001**, *9*, 709.
(3) Qu, Fanyao; Dantas, N. O.; Morais, P. C. *Europhys. Lett.* **2001**, *53*, 790.
(4) Qu, Fanyao; Morais, P. C. *J. Phys. Chem.* **2000**, *104*, 5232.
(5) Klimov, V. I.; Mikhailovsky, A. A.; McBranch, D. W.; Leatherdale, C. A.; Bawendi, M. C. *Science* **2000**, *287*, 101.
(6) Klimov, V. I.; Mikhailovsky, A. A.; Xu, Su; Malko, A.; Hollingsworth, J. A.; Leatherdale, C. A.; Eisler, H.-J.; Bawendi, M. C. *Science* **2000**, *290*, 314.
(7) Tsuyoshi, O.; Andrey, A. L.; Tomoyasu, O.; Isamu, A.; Yasuaki, M. *J. Lumin.* **2000**, *87−89*, 491.
(8) Thielsch, R.; Böhme, T.; Reiche, R.; Schläfer, D.; Bauer, H. D.; Böttcher, H. *Nanostruct. Mater.* **1998**, *10*, 13.
(9) Iino, T.; Weber, J. *Mater. Sci. Forum* **1995**, *196−201*, 993.
(10) Su, Z. P.; Teo, K. L.; Yu, P. Y.; Uchida, K. *Solid State Commun.* **1996**, *99*, 933.
(11) Seidel, W.; Tikov, A.; André, J. K.; Voisin, P.; Voos, M. *Phys. Rev. Lett.* **1994**, *73*, 2356.
(12) Vagos, P.; Boucaud, P.; Julien, F. H.; Lourtioz, J. M. *Phys. Rev. Lett.* **1993**, *70*, 1018.
(13) Hellmann, R.; Euteneuer, A.; Hense, S. G.; Feldmann, J.; Thomas, P.; Göbel, E. O. *Phys. Rev. B* **1995**, *51*, 18053.
(14) Junnarkar, M. R.; Yamaguchi, E. *Solid-State Electron.* **1996**, *40*, 665.
(15) Cheong, H. M.; Fkuegel, B.; Hanna, M. C.; Mascarenhas, A. *Phys. Rev. B* **1998**, *58*, R4254.
(16) Paskov, P. P.; Holtz, P. O.; Monemar, B.; Garcia, J. M.; Schoenfeld, W. V.; Petroff, P. M. *Appl. Phys. Lett.* **2000**, *77*, 812.
(17) Ignatiev, I. V.; Kozin, I. E.; Ren, H. W.; Sugou, S.; Masumoto, Y. *Phys. Rev. B* **1999**, *60*, R14001.
(18) Poles, E.; Selmarten, D. C.; Micic, O. I.; Nozik, A. J. *Appl. Phys. Lett.* **1999**, *75*, 971.
(19) Tudury, G. E.; Marquezini, M. V.; Ferreira, L. G.; Barbosa, L. C.; César, C. L. *Phys. Rev. B* **2000**, *62*, 7357.
(20) Andreev, A. D.; Lipovskii, A. A. *Phys. Rev. B* **1999**, *59*, 15402.
(21) Sales, F. V.; Da Silva, S. W.; Monte, A. F. G.; Soler, M. A. G.; Cruz, J. M. R.; Da Silva, M. J.; Quivy, A. A.; Leite, J. R.; Morais, P. C. *Phys. Status Solidi A* **2001**, *187*, 45.